Received: 29 December 2020 | Revised: 3 June 2021 | Accepted: 9 June 2021

DOI: 10.1111/joa.13493

Journal of Anatomy ANATOMICAL SOCIETY WILEY

ORIGINAL PAPER

Localization of nerve entry points and the center of intramuscular nerve-dense regions in the adult pectoralis major and pectoralis minor and its significance in blocking muscle spasticity

Yanrong Li[1] | Meng Wang[2] | Shaohua Tang[3] | Xiankun Zhu[4] | Shengbo Yang[2]

[1]Department of Radiology, Affiliated Hospital of Zunyi Medical University, Zunyi, China

[2]Department of Anatomy, Zunyi Medical University, Zunyi, China

[3]Department of Orthopaedics, Shijie Hospital, Dongguan, China

[4]Department of Rehabilitation, Zunyi Medical University, Zunyi, China

Correspondence
Shengbo Yang, Department of Anatomy, Zunyi Medical University, 6 West Xuefu Road, Xinpu Developing Zones, Zunyi 563099, China.
Email: yangshengbo8205486@163.com

Funding information
Science and technology projects of Guizhou Province, Grant/Award Number: ZK[2021]115; National Natural Science Foundation of China, Grant/Award Number: 31660294

Abstract

The aims of this study were to localize the body surface position and depth of nerve entry points, and the center of the intramuscular nerve-dense regions of the pectoralis major and pectoralis minor in order to provide guidance for blocking muscle spasticity. Formalin-fixed adult cadavers (66.3 ± 5.2 years) were used. The curved line on the skin from the acromion to the most inferior point of the jugular notch was defined as the horizontal reference line (H). The line from the most inferior point of the jugular notch to the xiphisternal joint was defined as the longitudinal reference line (L). The nerve entry points was anatomically exposed. Sihler's staining, barium sulfate labeling, and computed tomography were employed to determine the projection points (P) on the body surface. The intersection of the longitudinal line through the P point and the H line and the horizontal line through the P point and the L line were recorded as P_H and P_L, respectively. The projection of the nerve entry points or the center of the intramuscular nerve-dense regions were in the opposite direction across the transverse plane and were recorded as P'. The percentage positions of P_H and P_L on the H and L lines, as well as the nerve entry points and the center of the intramuscular nerve-dense regions depths, were determined using the Syngo system. The pectoralis major had two nerve entry points, while the pectoralis minor had only one. In addition, two intramuscular nerve-dense regions were found in the pectoralis major, while only one region was found in the pectoralis minor. The P_H of the nerve entry points were located at 47.83%, 32.31%, and 34.31%, while the P_H of the center of the intramuscular nerve-dense regions were at 41.95%, 55.88%, and 32.58% of line H, respectively. The P_L of the nerve entry points were at −9.84%, 36.16%, and 2.44%, while the P_L for each of three center of the intramuscular nerve-dense regions was at −3.87%, 25.29%, and −7.13% of line L, respectively. The depth for each of the nerve entry points was at 17.76%, 17.53%, and 25.51% of line P-P″, respectively, and the depth of the center of the intramuscular nerve-dense regions was at 5.23%, 6.75%, and 13.73% of line P-P′, respectively. These percentage values are all means. The

definition of the surface position and depth of these nerve entry points and center of the intramuscular nerve-dense regions can improve the localization efficiency and efficacy of target blocking for pectoralis major and minor spasticity.

KEYWORDS
center of intramuscular nerve-dense region, nerve entry point, pectoralis major, pectoralis minor, target localization

1 | INTRODUCTION

Muscle spasticity is often secondary to stroke, spinal cord injury, multiple sclerosis, head injury, and other central nervous system diseases. For stroke alone, the incidence exceeds 120/100,000, which suggests that many patients have muscle spasticity (Cabral et al., 2017; Lucchese et al., 2019). Once pectoralis major muscle and/or pectoralis minor muscle spasticity occur(s), patients will have shoulder joint adduction, rotation contracture, limited activity, and pain (Seruya & Johnson, 2016).

Neurotomy (Sindou et al., 2007), dry needling (Tang, Li, et al., 2018; Tang, Zhang, et al., 2018) tendon lengthening or release (Seruya & Johnson, 2016), extramuscular neurolysis, and intramuscular chemodenervation (Kaymak et al., 2019; Krylova & Khasanova, 2017) are clinically feasible to treat spasticity of the pectoralis major and pectoralis minor muscles. The latter two methods are more commonly used and relatively effective. Extramuscular neurolysis refers to the injection of ethanol or phenol into the nerve trunk or nerve entry point (NEP), which causes axonal degeneration and thereby reduces the activity of local muscles and nerves (Han et al., 2017). Intramuscular chemodenervation refers to the injection of botulinum toxin A (BTX-A) to the motor endplate, which blocks the release of acetylcholine from the presynaptic membrane and thereby inhibits muscle excitation (Pirazzini & Rossetto, 2017). These two methods can be assisted by palpation, electromyography, ultrasound, or an electrical stimulator to localize the target (Ahmed et al., 2016; Yi et al., 2017; Zeuner et al., 2017); however, these methods cannot accurately localize the surface position and puncture depth of the blocking target and cannot avoid the pain and certain unpleasant complications caused by exploratory punctures. Therefore, localizing the target accurately is necessary.

Many reports exist regarding the innervation and variation of pectoralis major and pectoralis minor muscles (Beheiry, 2012; Corten et al., 2003; Haladaj et al., 2019; Hoffman & Elliot, 1987; Macchi et al., 2007; Shetty et al., 2014). However, few reports exist regarding the location of targets for extramuscular and intramuscular nerve block. The gross anatomical location of the extramuscular nerve block point of the pectoralis major muscle has been described in one study (Sefa Özel et al., 2011). However, the study only described the medial and lateral relationship between the block point and the bony landmarks rather than the superior and inferior relationship and the puncture depth. The extramuscular nerve block point of the pectoralis minor muscle has not been located. For the localization of the intramuscular blocking points (i.e., motor endplate band) of the pectoralis major and pectoralis minor muscles, the staining of the motor endplate band may require fresh specimens, which has not been studied. Research has shown that the location of the intramuscular nerve-dense region (INDR) is consistent with the location of the motor endplate, which can be used as an alternative target for BTX-A (Amirali et al., 2007). The distribution pattern of the intramuscular nerves of the pectoralis major has been revealed by using Sihler's staining (Haladaj et al., 2019); however, its INDR has not been located.

Therefore, in this study, we aimed to expose the NEP by dissecting and displaying the INDR by using Sihler's staining, labeling the NEP and the center of the INDR (CINDR) with barium sulfate, and conducting spiral computed tomography (CT) scanning and three-dimensional reconstruction. With the help of bony landmarks, the body surface position and puncture depth of the NEP and CINDR can be accurately defined so as to provide guidance for the localization of blocking targets for muscle spasticity and to improve the efficiency and efficacy of target blocking.

2 | MATERIALS AND METHODS

2.1 | Specimens and ethics

Forty donated adult cadavers (26 men and 14 women, aged 30–75 (66.3 ± 5.2) years) of individuals without a neuromuscular disease history or chest and upper limb joint deformation were fixed with formalin. The causes of death of these donors were cancer, heart disease, or accidents. None of the cadaver donors were from a vulnerable population, and all donors or their next of kin provided signed written consent forms before being accepted for use in this project. The research protocol was preapproved by the Ethics Commission of Zunyi Medical University (Zunyi, China; approval no.: 2016-1-006).

2.2 | Gross anatomy observation

With the cadaver supine, the skin and subcutaneous fat were cut in the layer close to the surface of the muscle by using the following route: starting from the acromion and proceeding to the lowest point of the jugular vein incision, and then continuing through the xiphoid tip, costal arch, posterior axillary line, upper part of

the posterior axillary fold, upper part of the medial border of the arm, middle part of the medial border of the arm, middle part of the lateral border of the arm, and returning to the acromion. After exposing the deltoid and the pectoralis major muscles, as well as removing the origin of the pectoralis major muscle close to the clavicle, the lateral pectoral nerve and its branches were carefully identified and retained. The pectoral major muscle was reflected medioinferiorly, and the pectoralis minor muscle was exposed. The medial pectoral nerve and its pectoralis major muscle branches were carefully separated. The course of the nerve, the number of nerve branches, the site of nerve entering the muscle, and whether an accompanying blood vessel existed were observed. If more than one nerve branch was observed, thus indicating multiple NEPs, we defined the NEP of the thickest nerve branch as the target of study.

2.3 | Reference line design

The curved line close to the skin connecting the acromion (i.e., point a) and the most inferior point of the jugular notch (i.e., point b) was designed as the horizontal reference line (i.e., the H line). The curved line connecting the most inferior point of the jugular notch with the xiphisternal joint (i.e., point c) was designed as the longitudinal reference line (i.e., the L line).

2.4 | Spiral CT localization of the NEP

After the gross anatomical observation, the NEPs were labeled with barium sulfate mixed with glue and reset and sutured layer by layer. A barium sulfate-soaked silk thread was then sewn on the skin between the bony landmarks to represent the reference line. The sample was scanned with 16-row spiral CT (Siemens), and a three-dimensional image was reconstructed. The white spot (i.e., the NEP) labeled with barium sulfate was detected on the cross-section image. Under the same indicator light and with the aid of spiral CT scanning and percutaneous needle puncture perpendicular to the coronal plane, the projection point (i.e., the P point) of the NEP on the chest body surface was located (i.e., the body surface puncture point). The NEPs of the lateral pectoral nerve, the medial pectoral nerve innervating the pectoralis major, and the medial pectoral nerve innervating the pectoralis minor were named NEP_{1a}, NEP_{1b}, and NEP_2, respectively, and their P points were named P_{1a}, P_{1b}, and P_2, respectively. The intersection of the horizontal line through the P point and the L line was recorded as P_L (i.e., $P_{1a\text{-}L}$, $P_{1b\text{-}L}$, and P_{2L}), and the curve length between the most inferior point (point b) of the jugular notch and the P_L point was recorded as L′ (i.e., L_{1a}', L_{1b}', and L_2'). The intersection of the vertical line through point P and the H line was recorded as P_H (i.e., $P_{1a\text{-}H}$, $P_{1b\text{-}H}$, and P_{2H}). The length between the acromion (point a) and the P_H point was H′ (i.e., H_{1a}', H_{1b}' and H_2'), and was calculated as H′/H × 100% and as L′/L × 100%, respectively. It was determined as the percentage position of the NEP on the body surface. On the cross-section, the P point projecting to the back skin after passing through the NEP was defined as the P′ point, and the P-NEP and P-P′ were measured. The P-NEP/PP′ × 100% value was calculated, and the percentile puncture depth was determined. For NEP_{1b} in this experiment, only the depth in male individuals was measured because of individual differences in the female breast.

2.5 | Modified Sihler's staining to determine intramuscular nerve distribution

After localizing the NEP, the pectoralis major and pectoralis minor muscles of 20 cadavers were removed and underwent Sihler's staining procedure, based on our previous scheme (Luo et al., 2020; Tang, Li, et al., 2018; Tang, Zhang, et al., 2018; Wang et al., 2020; Yang et al., 2017). The samples were immersed in a solution of 3% potassium hydroxide and 0.2% hydrogen peroxide for 4 weeks, decalcified in Sihler's I solution for 4 weeks, and stained in Sihler's II solution for 4 weeks. The samples were then decolorized in Sihler's I solution for 2–10 h and neutralized in 0.05% lithium carbonate for 2 h. The gradient glycerin (40%, 60%, 80%, and 100%) was transparent for 1 week. The branch distribution of intramuscular nerve was observed on an X-ray reading box. The percentages of the INDR and CINDR in the muscle length (i.e., from the origin to the insertion) and in the muscle width (i.e., from the top to the bottom) were measured by using a Vernier caliper.

2.6 | Spiral CT localization of the CINDR

Based on the percentage position of CINDRs on the muscles measured in the aforementioned Sihler's staining procedure, the pectoralis major and pectoralis minor muscles of the remaining 20 cadavers (men, 13; women, 7) were dissected and exposed. The corresponding position of the CINDRs was located on these muscles, the CINDRs were labeled with barium sulfate mixed with glue. They were then sutured in situ layer by layer to undergo spiral CT localization of the CINDRs. The localization method of the CINDR was the same as that for the NEP. After localization, these muscles were removed and stained with Sihler's staining to verify whether the distribution pattern of the intramuscular nerves and the position of the CINDR were consistent with those of the previously stained muscle specimens.

2.7 | Statistical processing

The experimental data were processed by SPSS18.0 software (IBM) and expressed as a percentage ($\bar{x} \pm s$, %), thereby eliminating the influence of individual differences. The left and right sides were compared using the paired t test. The muscle samples of the men and the women were compared by using the t test. The test level was $\alpha = 0.05$.

3 | RESULTS

3.1 | Gross anatomy

The lateral pectoral nerve originated from the lateral cord of the brachial plexus and descended to the deep surface of the pectoralis major muscle through the lateral side of the midpoint of the clavicle, and before entering the muscle. It is usually divided into three branches (90%, 72/80 sides). These branches were in proximity with each other, and each branch had branches and tributaries of the thoracoacromial vessels running into the muscle. The NEP of the middle branch was the target of this study (Figure 1a). The medial pectoral nerve from the medial cord of the brachial plexus was on the lateral side of the lateral pectoral nerve and usually divided into three branches (92.5%, 74/80 sides) before entering the muscle. Among these three branches, one branch passed through the center of the superolateral one-third of the pectoralis minor muscle and reached the deep surface of the middle part of the pectoralis major muscle, while another branch entered the superior-middle part of the pectoralis minor muscle and the last branch, which was the smallest, passed through the inferolateral border of the pectoralis minor muscle and reached the inferolateral border of the pectoralis major muscle (the branch was not localized) (Figure 1b). In one cadaver, the clavicle part of the pectoralis major muscle was fused with the deltoid muscle (2.5%, 2/80 sides), and no deltopectoral groove and cephalic vein were found between the two muscles. The fourth intercostal nerve was involved in the innervation of the inferolateral pectoralis major muscle in 13.75% (11/80 sides) of the specimens.

3.2 | Spiral CT localization of the NEP

Tables 1 and 2 show the percentage position of the P_H point on line H, and the P_L point on line L of the pectoralis major branch of the lateral pectoral nerve, the pectoralis major branch of the medial pectoral nerve (in men only), the pectoral minor branch of the medial pectoral nerve, and the depth of NEP. The data were not significantly different between the left and right sides or between the men and women ($p > 0.05$). In Figure 2, the CT location image is illustrated by the location of the NEP in the pectoralis minor branch of the medial pectoral nerve.

3.3 | Intramuscular nerve distribution

After the three primary branches of the lateral pectoral nerve entered the pectoralis major muscle, two branches ran vertically with the muscle fibers in the clavicular part of the pectoralis major muscle and then gradually separated from each other from the deep side of the muscle to the superficial side. Along the way, a large number of small arborized branches were sent out, which were anastomosed with each other and formed an intramuscular nerve-dense region (i.e., $INDR_{1a}$). The other primary nerve branch ran to the center of the sternal part of the pectoralis major muscle. Many arborized branches were sent out, which were anastomosed with the branches of medial pectoral nerve, to form another intramuscular nerve-dense region (i.e., $INDR_{1b}$). After the medial pectoral nerve passed through the pectoralis minor muscle and entered the pectoralis major muscle, it ran superolaterally to inferomedially and its

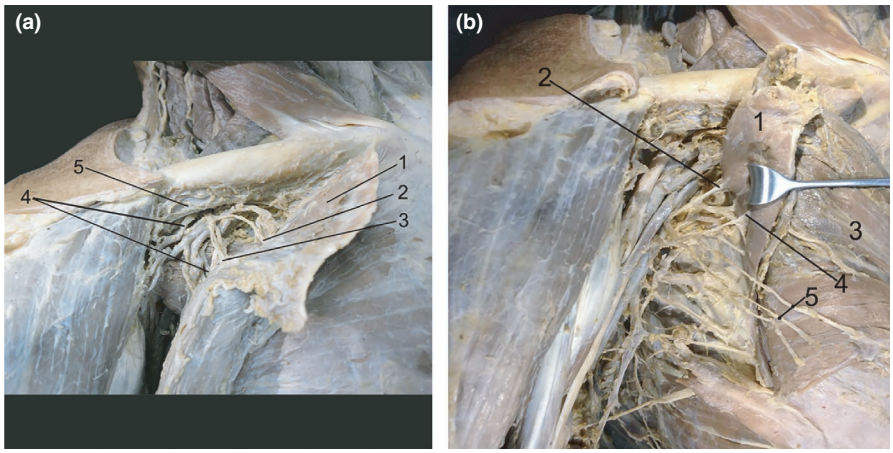

FIGURE 1 Gross anatomy of the nerve entry points of the pectoralis major and pectoralis minor. (a) Gross anatomy of the nerve entry points of the lateral pectoral nerve: "1" is the reflected pectoralis major muscle, "2" is the nerve entry point of the medial branch of the lateral pectoral nerve and accompanying vessels, "3" is the nerve entry point of the middle branch of lateral pectoral nerve and accompanying vessels, "4" is the nerve entry point of the lateral branch of the lateral pectoral nerve and accompanying vessels, and "5" is the subclavius muscle. (b) Gross anatomy of the nerve entry points of the medial pectoral nerve: 1" is the reflected pectoralis minor muscle, "2" is the branch of the medial pectoral nerve passing through the pectoralis minor muscle to the pectoralis major muscle, "3" is the nerve entry point of the pectoralis minor muscle branch of the medial pectoral nerve, "4" is the reflected pectoralis major muscle, and "5" is the small branch of the medial pectoral nerve passing through the inferolateral border of the pectoralis minor muscle to the inferolateral border of the pectoralis major muscle

TABLE 1 Comparison of the location of P_H and P_L of the NEPs on lines H and L respectively and depth of NEPs between the left and right sides in Pectoralis Major and Pectoralis Minor muscles (%) ($\bar{x} \pm s$, %, n = 20)

	P_H on H line (H′/H)				P_L on L line (L′/L)				Depth of NEP (P-NEP/PP′)			
NEP	Left	Right	*t*	*p*	Left	Right	*t*	*p*	Left	Right	*t*	*p*
NEP_{1a}	47.64 ± 0.60	47.70 ± 0.67	−0.510	0.616	−9.75 ± 0.24	−9.64 ± 0.25	−1.632	0.119	17.62 ± 0.60	17.52 ± 0.57	0.811	0.427
NEP_{1b}	32.12 ± 0.60	32.03 ± 0.46	0.666	0.513	36.14 ± 0.15	36.08 ± 0.32	0.606	0.552	17.42 ± 0.46	17.31 ± 0.67	0.912	0.373
NEP_2	34.43 ± 0.39	34.43 ± 0.59	−0.024	0.981	2.43 ± 0.17	2.46 ± 0.23	−0.585	0.565	25.58 ± 0.46	25.48 ± 0.61	0.809	0.429

Abbreviation: NEP, nerve entry point.

TABLE 2 Comparison of the location of P_H and P_L of the NEPs on lines H and L, respectively, and depth of NEPs between the male and female in pectoralis major and pectoralis minor muscles (%) ($\bar{x} \pm s$, %)

	P_H on H line (H′/H)				P_L on L line (L′/L)				Depth of NEP (P-NEP/PP′)			
NEP	Male (*n* = 13)	Female (*n* = 7)	*t*	*p*	Male (*n* = 13)	Female (*n* = 7)	*t*	*p*	Male (*n* = 13)	Female (*n* = 7)	*t*	*p*
NEP_{1a}	47.60 ± 0.55	47.81 ± 0.75	−1.006	0.229	−9.67 ± 0.24	−9.73 ± 0.26	0.700	0.901	17.53 ± 0.62	17.66 ± 0.52	−0.660	0.326
NEP_{1b}	—	—	—	—	—	—	—	—	—	—	—	—
NEP_2	34.47 ± 0.54	34.37 ± 0.40	0.624	0.227	2.43 ± 0.22	2.48 ± 0.18	−0.676	0.584	25.56 ± 0.60	25.49 ± 0.41	0.352	0.160

Abbreviation: NEP, nerve entry point.

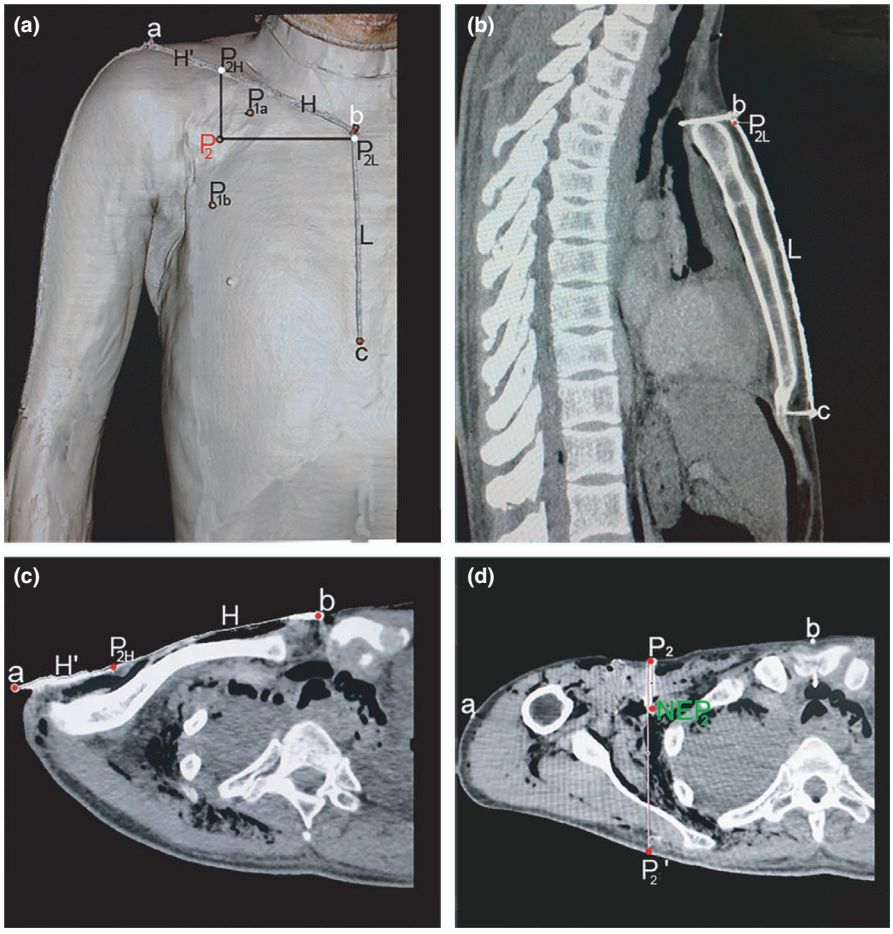

FIGURE 2 Computed tomography localization of the medial pectoral nerve entry point (NEP_2) innervating the pectoralis minor muscle. (a) The position of the NEP projection on the body surface and the design reference line. P_{1a} and P_{1b} represent the projection points of the lateral pectoral nerve and the medial pectoral nerve NEP on the body surface, respectively. P_2 is the projection point of NEP_2 on the body surface of the chest. (b) Measurement of the length of the L and L′ lines in the sagittal section. (c) Measurement of the length of the H and H′ lines on the cross-section through the H line. (d) Measurement of the depth of the NEP_2 on the cross-section through P_2

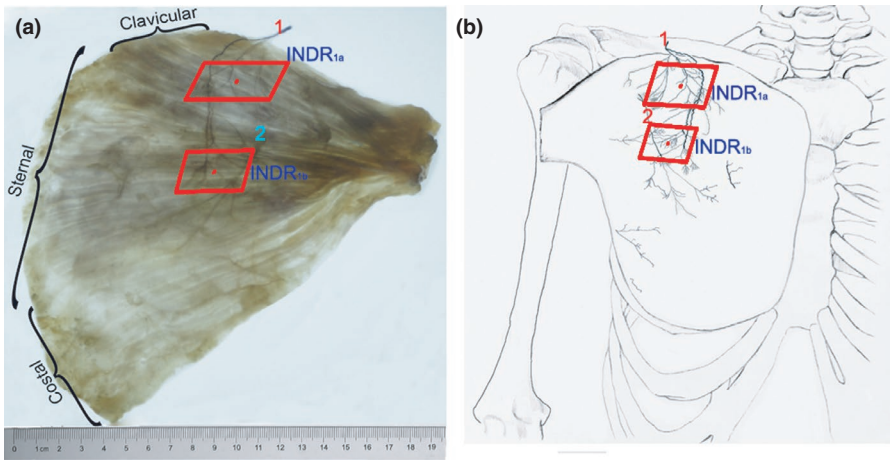

FIGURE 3 Distribution pattern of the intramuscular nerves in the right pectoralis major and the position of the INDR (deep view). (a) Sihler's staining results: "1" is the lateral pectoral nerve and "2" is the medial pectoral nerve. The red boxes represent the INDRs and the red dots represent the CINDRs. Scale, cm. (b) Schematic drawing of (a) and the positions of the INDRs and CINDRs in the muscle. INDR, intramuscular nerve-dense region; CINDR, center of the intramuscular nerve-dense region

arborized branches were distributed to the sternal and costal part of the pectoralis major muscle. The small branches of the medial pectoral nerve, which entered the muscle from the inferolateral border of the pectoralis major, were distributed in the costal part of the pectoralis major. Figure 3 and Table 3 present the area of the two nerve-dense regions in the muscle and the position of the CINDR in the muscle.

After the medial pectoral nerve entered the pectoralis minor muscle, it usually divided into the medial and lateral primary branches, each of which was further divided into three to four secondary branches at 28.36% of the muscle length. The lateral secondary branch and its arborized branches mostly ran to the lateral border of the muscle, and some branches ran to the origin end of the muscle. The secondary branches of the medial side fanned out the tertiary and the following branches, which ran between the muscle bundles. The branches were concentrated at the 28.36%–46.45% level of the muscle length. Together with the branches of the primary branches of the medial side, these branches formed a dense region (i.e., $INDR_2$) with more "U-shaped" anastomoses. The size of the region and the position of the CINDR in the muscle are shown in Figure 4 and Table 3. After the specimens that had undergone spiral CT localization of CINDR were stained with Sihler's staining, we noticed that the intramuscular nerve distribution pattern and the CINDR location were consistent with those of the previous specimens stained with Sihler's staining.

TABLE 3 The area of INDRs and location of CINDRs on muscle length and width ($\bar{x} \pm s$, %, n = 20)

INDR	Area (cm^2)	CINDR on muscle length (%)	CINDR on muscle width (%)
$INDR_{1a}$	10.42 ± 0.28	60.33 ± 0.71	18.84 ± 0.52
$INDR_{1b}$	6.15 ± 0.36	55.63 ± 0.75	56.96 ± 0.86
$INDR_2$	9.02 ± 0.37	34.07 ± 0.59	45.05 ± 0.69

Abbreviations: CINDR, center of intramuscular nerve dense region; INDR, intramuscular nerve dense region.

3.4 | The location of the CINDR based on CT

Tables 4 and 5 show the surface percentage position of the P_H and P_L point of the two CINDRs of the pectoralis major muscle and one CINDR of the pectoralis minor muscle projecting on the H and L lines and the percentage depth of the CINDR. In Figure 5, the CT localization image of the CINDR is represented by the CINDR localization of the second INDR in the pectoralis major muscle. The data between the left side and right sides or between the men and women were not statistically difference ($p > 0.05$).

4 | DISCUSSION

In this study, we aimed to accurately localize the body surface position and depth of the NEPs and the CINDRs of the pectoralis major and pectoralis minor by using Sihler's staining, barium sulfate labeling, and CT scanning. By using these techniques, we were able to

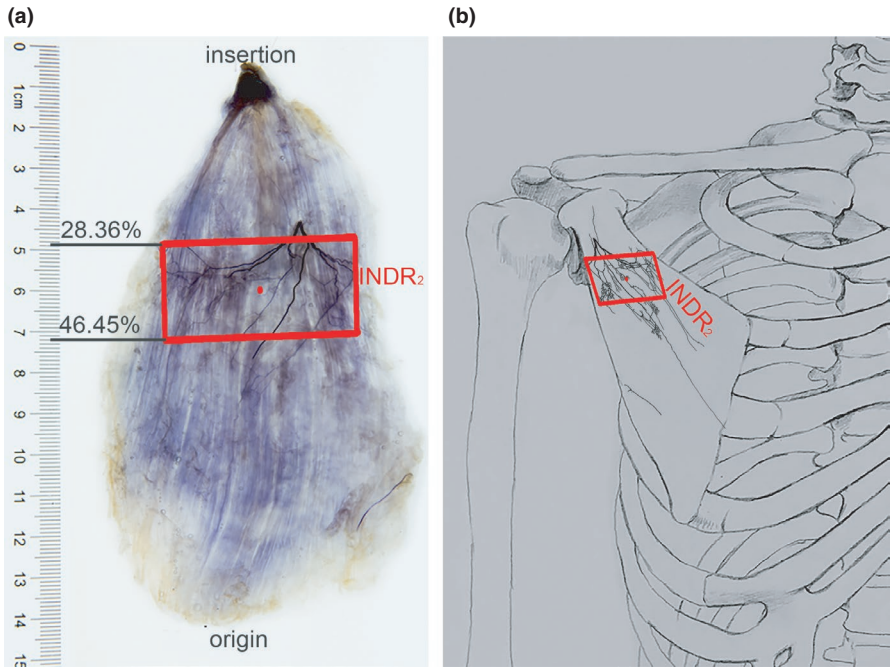

FIGURE 4 Distribution pattern of the intramuscular nerves in the right pectoralis minor and the position of the INDR (deep view). (a) Sihler's staining. Scale, cm. The red box indicates the INDR and the red dot indicates the CINDR. (b) Schematic drawing of (a) and the positions of the INDR and CINDR in the muscle. INDR, intramuscular nerve-dense region; CINDR, center of the intramuscular nerve-dense region

TABLE 4 Comparison of the location of P_H and P_L of the CINDRs on lines H and L respectively and depth of CINDRs between the left and right sides in pectoralis major and pectoralis minor muscles (%) ($\bar{x} \pm s$, %, n = 20)

	P_H on H line (H'/H)				P_L on L line (L'/L)				Depth of CINDRs (P-CINDR/PP')			
CINDR	Left	Right	*t*	*p*	Left	Right	*t*	*p*	Left	Right	*t*	*p*
$CINDR_{1a}$	41.96 ± 0.52	41.96 ± 0.72	−0.042	0.967	−3.92 ± 0.51	−3.89 ± 0.49	−0.462	0.649	5.24 ± 0.52	5.33 ± 0.48	−1.268	0.220
$CINDR_{1b}$	55.86 ± 0.54	55.81 ± 0.53	1.001	0.329	25.27 ± 0.54	25.19 ± 0.66	0.962	0.348	6.73 ± 0.54	6.66 ± 0.66	0.950	0.354
$CINDR_2$	32.48 ± 0.56	32.37 ± 0.54	1.319	0.203	−6.98 ± 0.48	−6.97 ± 0.51	−0.088	0.931	13.63 ± 0.56	13.64 ± 0.54	−0.029	0.977

Abbreviation: CINDR, center of intramuscular nerve dense region.

TABLE 5 Comparison of the location of P_H and P_L of the CINDRs on lines H and L respectively and depth of CINDRs between the male and female in pectoralis major and pectoralis minor muscles (%) ($\bar{x} \pm s$, %)

	P_H on H line (H'/H)				P_L on L line (L'/L)				Depth of CINDRs (P-CINDR/PP')			
CINDR	Male (n = 13)	Female (n = 7)	*t*	*p*	Male (n = 13)	Female (n = 7)	*t*	*p*	Male (n = 13)	Female (n = 7)	*t*	*p*
$CINDR_{1a}$	42.07 ± 0.58	41.76 ± 0.70	1.515	0.826	−3.95 ± 0.51	−3.81 ± 0.47	−0.881	0.438	5.35 ± 0.53	5.17 ± 0.41	1.101	0.264
$CINDR_{1b}$	55.91 ± 0.55	55.70 ± 0.48	1.195	0.823	25.31 ± 0.63	25.07 ± 0.51	1.240	0.721	6.76 ± 0.65	6.58 ± 0.48	0.904	0.357
$CINDR_2$	32.44 ± 0.54	32.41 ± 0.59	0.143	0.731	−7.04 ± 0.45	−6.87 ± 0.56	−1.078	0.384	13.66 ± 0.55	13.59 ± 0.54	0.426	0.546

Abbreviation: CINDR, center of intramuscular nerve dense region.

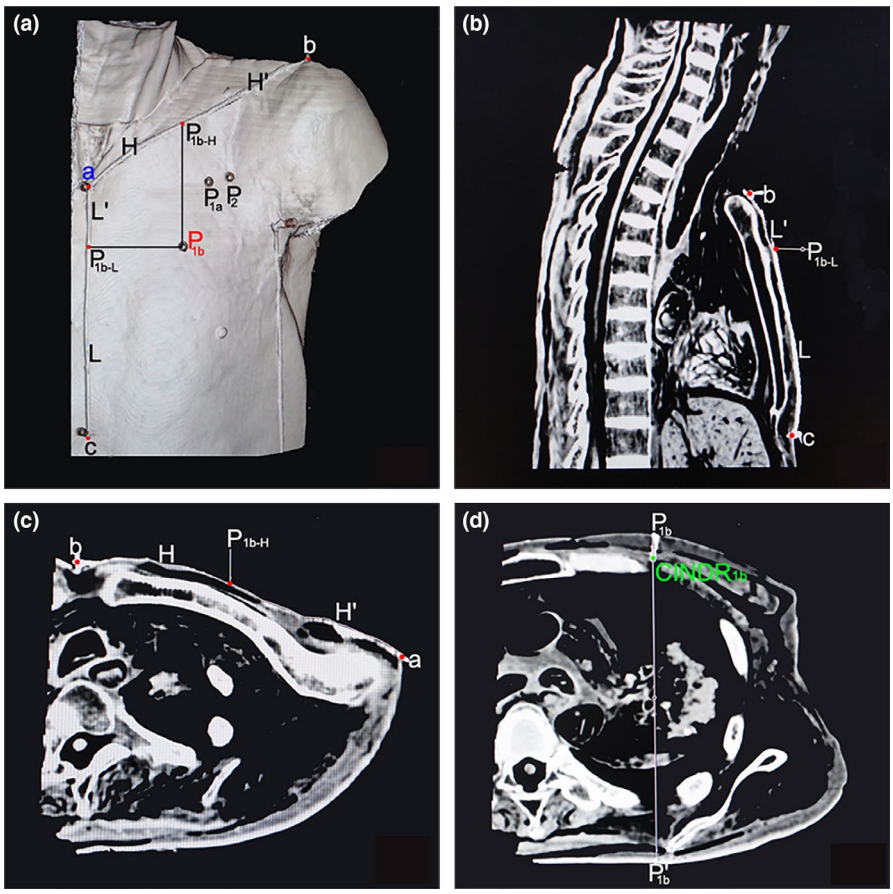

FIGURE 5 Computed tomography localization of $CINDR_{1b}$ in the pectoralis major muscle. (a) The position of $CINDR_{1b}$ on the body surface (P_{1b}) and the designed reference line. (b) The length of the L and L′ lines measured on the sagittal section. (c) The length of the H and H′ lines measured on the cross-section. (d) The depth of $CINDR_{1b}$, measured on the cross-section

detect more readily the positions of the NEP and CINDR in these muscles. Injecting phenol or ethanol into the intramuscular nerve trunk to block muscle spasticity will cause non-spastic muscle involvement and paresthesia. The NEPs are located closer to motor end-plate and blocking them requires shorter axonal regenerative time. Thus, blocking the NEPs is conducive to the recovery of muscle function (Yang et al., 2017). The intramuscular injection of BTX-A to the motor endplate or to the INDR to block muscle spasticity has become increasingly popular (Tang, Li, et al., 2018; Tang, Zhang, et al., 2018; Yang et al., 2017). Injecting BTX-A to block the spasticity of the pectoralis major muscle is the most commonly used method to treat hemiplegic shoulder pain (Holmes & Connell, 2019). For the pectoralis minor muscle, BTX-A injection can also treat outlet syndrome (Rahman et al., 2019). However, the surface location and puncture depth of NEP and CINDR have not been defined. Therefore, accurately locating the anatomical details of the NEP and CINDR of pectoralis major and pectoralis minor is necessary.

Previous studies have investigated the location of the nerve trunk to block the spasticity of pectoralis major muscle. Sefa Özel et al. (2011) used the long axis of the clavicle as the horizontal reference line and the median line of the sternum as the longitudinal reference line. They found that the best blocking target for the lateral pectoral nerve was at the intersection of the vertical line through the junction of the medial and middle one-third of the clavicle and the horizontal line through the most inferior point of the jugular notch. Our study found that no lateral pectoral nerves originating from the brachial plexus descended from the deep side of the junction of the medial and the middle one-third of the clavicle, but instead descended from the deep side lateral to the midpoint of the clavicle. Behringer et al. (2014) used electrical stimulation to locate the motor points of the pectoralis major and pectoralis minor muscles. The *y*-axis reference line was from the most inferior point of the jugular notch to the xiphisternal joint, and the horizontal line of the most inferior point of the jugular notch was the *x*-axis reference line. The motor points were located respectively at 42.86% and 71.56% of the *x*-axis and at 17.05% and 14.39% of the *y*-axis (Behringer et al., 2014). A limitation of these useful studies is that they did not involve the depth of puncture.

Based on current research, the following factors are worth mentioning: (1) blood vessels are near the NEP of the pectoralis major and pectoralis minor (thus, when injecting drugs, the syringe piston should be pulled back to prevent the drugs from entering the blood

vessels by mistake) and (2) the NEP of the pectoralis major branch of the medial pectoral nerve is below the level of the third rib, which is lower than the upper limit of the breast (i.e., the second rib), individual differences in breast size is large, and the thoracic wall depth differs between men and women. Therefore, in female patients with pectoralis major spasticity, the CINDR block is recommended as the first choice. If an NEP block is needed, the NEP of lateral pectoral nerve can be blocked (3). In this study, variations in the atrophied clavicle part of the pectoralis major muscle, as described by Haladaj et al. (2019), were not observed, but the fusion of the clavicle part of the pectoralis major muscle and the deltoid muscle, as described by Haladaj, was observed. The fourth intercostal nerve (13.75%) was involved in the innervation of the lower lateral pectoralis major muscle, which was consistent with Beheiry's description (Beheiry, 2012).

A BTX-A injection to block muscle spasticity is a dose-dependent chemical denervation. Once BTX-A is injected into the muscle, it will immediately spread within a few centimeters near the needle tip. If the position of the BTX-A injection point deviates from the motor endplate by 5 mm, this deviation will directly reduce the antispasmodic effect by 50% (Borodic et al., 1994). Within a certain range, appropriately increasing the drug dose can improve the treatment effect. However, the long-term use of a large dose will cause local muscle fibrosis and excessive muscle relaxation. Repeated injections can cause pain in patients and reduce or eliminate the effect of BTX-A (Parratte et al., 2002). Therefore, an appropriate amount of BTX-A should be accurately injected into the target site. Some studies have shown that a BTX-A injection of 1 unit can infiltrate 1.5–3.0 cm, whereas an injection of 2.5–5 units can diffuse 4.5 cm (Borodic et al., 1994; Holmes & Connell, 2019; Tang, Li, et al., 2018; Tang, Zhang, et al., 2018). At present, the clinical application doses of BTX-A for the pectoralis major and pectoralis minor are 100–500 units and 30–40 units, respectively (Kong et al., 2007; Marco et al., 2007). Based on the calculation of the INDR in this study, only 9–18 units were needed for the pectoralis major and 5–10 units were needed for the pectoralis minor. This result suggests that if the target location is accurate, the required dose of BTX-A will be greatly reduced, which is conducive to saving costs and reducing adverse effects.

In general, a geometric relationship between the NEP and CINDR and bony landmarks was established, and their body surface position and puncture depth were obtained by using barium sulfate labeling of the NEP and CINDR, spiral CT scanning, and three-dimensional reconstruction. Thus, morphological guidance was provided for the clinical treatment of spasticity of these two muscles and may improve the efficiency and efficacy of the target block. We suggest that the combination of an electrical stimulator and ultrasound can reduce the number of exploratory punctures and avoid puncturing the chest. However, some limitations exist in the present study such as the relatively small number of samples and the location of the NEP could not be fully used in female patients, which need further study. The real efficacy remains to be clinically verified.

ACKNOWLEDGMENTS

The authors would like to acknowledge Xufeng Tian for their excellent technical assistance and for the use of their spiral CT laboratory.

CONFLICT OF INTEREST

None.

AUTHOR CONTRIBUTIONS

Conception and design, acquisition of data, or analysis and interpretation of data: SY, YL, MW, ST, and XZ. Drafting the article or revising it critically for important intellectual content: YL, SY, and MW. All authors made direct and intellectual contribution to the work and approved it for publication.

DATA AVAILABILITY STATEMENT

Research data are not shared.

ORCID

Shengbo Yang https://orcid.org/0000-0003-0784-1008

REFERENCES

Ahmed, A., Arora, D. & Kochhar, A.K. (2016) Ultrasound-guided alcohol neurolysis of lateral femoral cutaneous nerve for intractable meralgia paresthetica: a case series. *British Journal of Pain*, 10(4), 232–237.

Amirali, A., Mu, L., Gracies, J.M. & Simpson, D.M. (2007) Anatomical localization of motor endplate bands in the human biceps brachii. *Journal of Clinical Neuromuscular Disease*, 9(2), 306–312.

Beheiry, E.E. (2012) Innervation of the pectoralis major muscle: anatomical study. *Annals of Plastic Surgery*, 68(2), 209–214.

Behringer, M., Franz, A., McCourt, M. & Mester, J. (2014) Motor point map of upper body muscles. *European Journal of Applied Physiology*, 114(8), 1605–1617.

Borodic, G.E., Ferrante, R., Pearce, L.B. & Smith, K. (1994) Histologic assessment of dose-related diffusion and muscle fiber response after therapeutic botulinum atoxin injections. *Movement Disorders*, 9(1), 31–39.

Cabral, N.L., Freire, A.T., Conforto, A.B., dos Santos, N., Reis, F.I., Nagel, V. et al. (2017) Increase of stroke incidence in young adults in a middle-income country: a 10-year population-based study. *Stroke*, 48(11), 2925–2930.

Corten, E.M., Schellekens, P.P., Bleys, R.L. & Kon, M. (2003) The nerve supply to the clavicular part of the pectoralis major muscle: an anatomical study and clinical application of the function-preserving pectoralis major island flap. *Plastic and Reconstructive Surgery*, 112(4), 969–975.

Haładaj, R., Wysiadecki, G., Clarke, E., Polguj, M. & Topol, M. (2019) Anatomical variations of the pectoralis major muscle: notes on their impact on pectoral nerve innervation patterns and discussion on their clinical relevance. *BioMed Research International*, 2, 6212039.

Han, K.R., Chae, Y.J., Lee, J.D. & Kim, C. (2017) Trigeminal nerve block with alcohol for medically intractable classic trigeminal neuralgia: long-term clinical effectiveness on pain. *International Journal of Medical Sciences*, 14(1), 29–36.

Hoffman, G.W. & Elliot, L.F. (1987) The anatomy of the pectoral nerves and its significance to the general and plastic surgeon. *Annals of Surgery*, 205(5), 504–507.

Holmes, R.J. & Connell, L.A. (2019) A survey of the current practice of intramuscular Botulinum toxin injections for hemiplegic shoulder pain in the UK. *Disability and Rehabilitation*, 41(6), 720–726.

Kaymak, B., Kara, M., Gürçay, E., Aydin, G. & Özçakar, L. (2019) Selective peripheral neurolysis using high frequency ultrasound imaging: a novel approach in the treatment of spasticity. *European Journal of Physical and Rehabilitation Medicine*, 55(4), 522–525.

Kong, K.H., Neo, J.J. & Chua, K.S. (2007) A randomized controlled study of botulinum toxin A in the treatment of hemiplegic shoulder pain associated with spasticity. *Clinical Rehabilitation*, 21(1), 28–35.

Krylova, L.V. & Khasanova, D.R. (2017) The features of botulinum therapy for different patterns of poststroke spasticity. *Zhurnal nevrologii i psikhiatrii im. S.S. Korsakova*, 117(2), 42–48.

Lucchese, G., Flöel, A. & Stahl, B. (2019) Cross-reactivity as a mechanism linking infections to stroke. *Frontiers in Neurology*, 14(10), 469.

Luo, H., Ji, S. & Yang, S. (2020) Localization of the centers of intramuscular nerve dense regions of the rotator cuff muscles: a guide for botulinum toxin A injection for spasticity accompanied by shoulder pain. *International Journal of Morphology*, 38(2), 435–443.

Macchi, V., Tiengo, C., Porzionato, A., Parenti, A., Stecco, C., Mazzoleni, F. et al. (2007) Medial and lateral pectoral nerves: course and branches. *Clinical Anatomy*, 20(2), 157–162.

Marco, E., Duarte, E., Vila, J., Tejero, M., Guillen, A., Boza, R. et al. (2007) Is botulinum toxin type A effective in the treatment of spastic shoulder pain in patients after stroke? A double-blind randomized clinical trial. *Journal of Rehabilitation Medicine*, 39(6), 440–447.

Parratte, B., Tatu, L., Vuillier, F., Diop, M. & Monnier, G. (2002) Intramuscular distribution of nerves in the human triceps surae muscle: anatomical bases for treatment of spastic drop foot with botulinum toxin. *Surgical and Radiologic Anatomy*, 24(2), 91–96.

Pirazzini, M. & Rossetto, O. (2017) Challenges in searching for therapeutics against botulinum neurotoxins. *Expert Opinion on Drug Discovery*, 12(5), 497–510.

Rahman, A., Hamid, A., Inozemtsev, K. & Nam, A. (2019) Thoracic outlet syndrome treated with injecting botulinum toxin into middle scalene muscle and pectoral muscle interfascial planes: a case report. *A&A Practice*, 12(7), 235–237.

Sefa Özel, M., Özel, L., Toros, S.Z., Marur, T., Yıldırım, Z., Erdoğdu, E. et al. (2011) Denervation point for neuromuscular blockade on lateral pectoral nerves: a cadaver study. *Surgical and Radiologic Anatomy*, 33(2), 105–108.

Seruya, M. & Johnson, J.D. (2016) Surgical treatment of pediatric upper limb spasticity: the shoulder. *Seminars in Plastic Surgery*, 30(1), 45–50.

Shetty, P., Nayak, S.B., Kumar, N., Thangarajan, R. & D'Souza, M.R. (2014) Origin of medial and lateral pectoral nerves from the supraclavicular part of brachial plexus and its clinical importance – a case report. *Journal of Clinical and Diagnostic Research*, 8(2), 133–134.

Sindou, M.P., Simon, F., Mertens, P. & Decq, P. (2007) Selective peripheral neurotomy (SPN) for spasticity in childhood. *Child's Nervous System*, 23(9), 957–970.

Tang, L., Li, Y., Huang, Q.M. & Yang, Y. (2018) Dry needling at myofascial trigger points mitigates chronic post-stroke shoulder spasticity. *Neural Regeneration Research*, 13(4), 673–676.

Tang, S., Zhang, X.M. & Yang, S. (2018) Localization of center of intramuscular nerve dense regions in adult anterior brachial muscles: a guide for botulinum toxin A injection to treat muscle spasticity. *American Journal of Translational Research*, 10(4), 1220–1228.

Wang, J., Wang, Q., Zhu, D., Jiang, Y. & Yang, S. (2020) Localization of the center of the intramuscular nerve dense region of the medial femoral muscles and the significance for blocking spasticity. *Annals of Anatomy - Anatomischer Anzeiger*, 231, 151529.

Yang, S., Hu, S., Li, B. & Li, X. (2017) Localization of nerve entry point and intramuscular nerve-dense regions as targets to block brachioradialis muscle spasticity. *International Journal of Clinical and Experimental Medicine*, 10(8), 11912–11920.

Yi, K.H., Cong, L., Bae, J.H., Park, E.S., Rha, D.W. & Kim, H.J. (2017) Neuromuscularstructure of the tibialis anterior muscle for functional electrical stimulation. *Surgical and Radiologic Anatomy*, 39(1), 77–83.

Zeuner, K.E., Knutzen, A., Kühl, C., Möller, B., Hellriegel, H., Margraf, N.G. et al. (2017) Functional impact of different muscle localization techniques for botulinum neurotoxin A injections in clinical routine management of post-stroke spasticity. *Brain Injury*, 31(1), 75–82.

How to cite this article: Li, Y., Wang, M., Tang, S., Zhu, X. & Yang, S. (2021) Localization of nerve entry points and the center of intramuscular nerve-dense regions in the adult pectoralis major and pectoralis minor and its significance in blocking muscle spasticity. *Journal of Anatomy*, 239, 1123–1133. https://doi.org/10.1111/joa.13493